Xiaoxia Yin · Brian W.-H. Ng
Derek Abbott

Terahertz Imaging for Biomedical Applications

Pattern Recognition and Tomographic Reconstruction

Springer

Terahertz Imaging for Biomedical Applications

Xiaoxia Yin • Brian W.-H. Ng • Derek Abbott

Terahertz Imaging for Biomedical Applications

Pattern Recognition and Tomographic Reconstruction

Springer

Dr. Xiaoxia Yin
School of Electrical and Electronic Engineering
University of Adelaide
Adelaide, Australia

Dr. Brian W.-H. Ng
School of Electrical and Electronic Engineering
University of Adelaide
Adelaide, Australia

Prof. Derek Abbott
School of Electrical and Electronic Engineering
University of Adelaide
Adelaide, Australia

Additional material to this book can be downloaded from http://extras.springer.com

ISBN 978-1-4614-1820-7 e-ISBN 978-1-4614-1821-4
DOI 10.1007/978-1-4614-1821-4
Springer New York Dordrecht Heidelberg London

Library of Congress Control Number: 2012930046

Printed on acid-free paper

Springer is part of Springer Science+Business Media (www.springer.com)

Preface

Over the last decade, terahertz (THz or T-ray) biomedical imaging has become a modality of interest due to its ability to simultaneously acquire both image and spectral information. THz imaging systems are being commercialized, with increasing interest in a biomedical setting. Advanced digital image processing algorithms are greatly needed to assist screening, diagnosis, and treatment. Pattern recognition algorithms play a critical role in the accurate and automatic process of detecting abnormalities when applied to biomedical imaging. This goal requires classification of information-bearing physical contrast patterns and identification of information in images, for example, distinguishing between different biological tissues or materials. T-ray tomographic imaging and detection technology contributes especially to our ability for discriminating opaque objects with clear boundaries and makes possible significant potential applications in both *in vivo* and *ex vivo* environments.

This monograph consists of a number of chapters, which can be grouped into three parts. The first part provides a review of the state-of-the-art regarding THz sources and detectors, THz imaging modes, and THz imaging analysis. Pattern recognition forms the second part of this monograph, which is represented via combining several basic operations: wavelet transforms and wavelet-based signal filtering, feature extraction and selection, along with classification schemes for THz applications. Signal filtering in this monograph is achieved via wavelet-based denoising. The ultrafast pulses generated by terahertz time-domain spectroscopic (THz-TDS) systems, are appropriate for decomposition in the wavelet domain as this can provide better denoising performance. Feature extraction and selection of the THz measurements rely on observed changes in pulse amplitude and phase, as well as scattering characteristics. Additionally, three signal processing algorithms are adopted for the evaluation of the complex insertion loss (CIL) function for example such as lactose, mandelic acid, and DL-mandelic acid: (a) standard evaluation by ratioing the sample with the background spectra, (b) a subspace identification algorithm, and (c) a novel wavelet packet identification procedure. These system identification algorithms enable THz measurements to be transformed to features for THz pattern recognition. Moreover, a feature extraction method

involving the use of AR and ARMA models on the wavelet transforms of measured T-ray pulse responses of ex vivo osteosarcoma cells as well as other biomedical materials is detailed. Classification schemes are carried out via simple and robust schemes, such as the linear Mahalanobis distance classifier and the nonlinear support vector machine (SVM) classifier. In particular, SVMs are used as a learning scheme to achieve the identification of two classes of RNA samples and multiple classes of powered materials.

The past decade has witnessed the tremendous development of THz instruments for detecting, storing, analyzing, and displaying images. THz-TDS is a broadband technique that generates and detects THz radiation in a synchronous and coherent manner. By contrast, the newly developed THz quantum cascade laser (QCL) is a narrowband radiation source that provides potential for realizing compact systems, producing image data with higher average power levels. The third part of this monograph discusses methods to improve the capability of both broad- and narrowband THz imaging, driven by computer-aided analytical techniques. A wavelet-based reconstruction algorithm for terahertz computed tomography (THz-CT) is represented to show how this algorithm can be used to rapidly reconstruct the region of interest (ROI) with a reduction in the measurements of terahertz responses, compared with a standard filtered back-projection technique. These reconstruction algorithms are applied to the analysis of acquired experimental data and to locally recover the two-dimensional (2D) and three-dimensional (3D) structures of several optically opaque objects. Moreover, a segmentation technique based on two-dimensional wavelet transforms is investigated for the identification of different materials from the reconstructed CT image.

Adelaide, Australia

Xiaoxia Yin
Brian W.-H. Ng
Derek Abbott

Acknowledgements

We wish to thank Dr. Bradley S. Ferguson (Tenix—Electronic Systems Division, now at Raytheon) for providing pulse CT data and Dr. Bernd M. Fischer for providing the RNA data. Thanks are due to Dr. Samuel P. Mickan for useful discussions. Many thanks to Prof. Sillas Hadjiloucas (Cybernetics, School of Systems Engineering, The University of Reading) for discussions and interaction in the area of signal processing techniques. Special thanks to Prof. Lynn Gladden (Head of Department of Chemical Engineering, University of Cambridge) and Dr. J. Axel Zeitler (Department of Chemistry, University of Cambridge) for their input on the THz QCL imaging aspects. In addition, we would like to express our appreciation to Prof. Xi-Cheng Zhang (J. Erik Jonsson Distinguished Professor, Director, Center for Terahertz Research at the Rensselaer Polytechnic Institute) for much inspiration and useful interaction.

Adelaide, Australia

Xiaoxia Yin
Brian W.-H. Ng
Derek Abbott

Contents

Acronyms

The following conventions have been adopted in this monograph:

1. *Definitions.* The T-ray band is defined in this monograph to span from 0.1 to 10 THz (THz$= 10^{12}$ Hz). This is an emerging definition in the literature. The T-ray band overlaps a little with the millimeter wave band (at lower T-ray frequencies) and the far-infrared band (at higher T-ray frequencies).
2. *Notation.* The acronyms and symbols used in this monograph are defined in the Glossary on p. 403. Standard abbreviations are used for the order of magnitude: T, tera-, 10^{12}; G, giga-, 10^{9}; M, mega-, 10^{6}; k, kilo-, 10^{3}; m, milli-, 10^{-3}; μ, micro-, 10^{-6}; n, nano-, 10^{-9}; p, pico-, 10^{-12}; f, femto-, 10^{-15}.
3. *Units.* All T-ray electric field amplitude data in this monograph is expressed in arbitrary units (AU). This means that the amplitude of the T-ray electric field has been normalized to a peak measurement, or to another reference measurement on the same system, depending on the experiment.
4. *Spelling.* Australian English spelling conventions have been used, as defined in the Macquarie English Dictionary (A. Delbridge (Ed.), Macquarie Library, North Ryde, NSW, Australia, 2001).
5. *Diagram colors.* The following color scheme is approximately followed in the diagrams:

    - Blue: T-ray beams—T-rays are invisible to the naked eye.
    - Red: laser beams — the majority of laser beam sources appearing in the diagrams are from optical femtosecond lasers.
    - Yellow: motion stages and samples—motion stages represent moving equipment, and samples can be composed of a wide variety of substances.
    - Orange: electrooptic and semiconductor crystals—these are typically T-ray sources and detectors.
    - Black/white: equipment, including optical components such as lenses and beam splitters.

Chapter 1
Introduction and Motivation to Terahertz Radiation

Terahertz pattern recognition is a signal processing procedure for extracting information from THz spectroscopic data. This is an area of study that is intimately tied to the measurement of terahertz data sets.

A challenge for THz pattern recognition systems is to explore the available methods for the identification of specific materials based on the THz responses. Most molecules show very complicated THz absorption spectra with a multitude of absorption lines. Those absorption lines are subject to thermal broadening at room temperature and are produced by classical electromagnetic interactions (Born and Wolf (2002) Principles of Optics: Electromagnetic Theory of Propagation, Interference and Diffraction of Light, Seventh Edition, Cambridge University Press, Cambridge, UK). Some of the traditional spectral analysis methods, for example, infrared spectroscopy, have greater Rayleigh scattering and are unable to access lower frequency vibrational modes, which motivates the current THz work.

This book describes several novel pattern recognition algorithms, which are applied to measured THz data. An algebraic reconstruction algorithm based on wavelet transforms of a local image is also presented. Moreover, since THz sources and detectors have developed to a point where high signal-to-noise ratio (SNR) and reasonable acquisition rates are possible, the combination of two-dimensional and three-dimensional imaging with spectroscopic information capture is an important elaboration of the current THz imaging system.

1.1 Introduction

This chapter introduces the field of THz (T-ray) spectroscopy and discusses the motivation for this area in respect of THz imaging and identification systems. It provides a road map for this book and a concise summary of the techniques of interest to the reader.

X. Yin et al., *Terahertz Imaging for Biomedical Applications: Pattern Recognition and Tomographic Reconstruction*, DOI 10.1007/978-1-4614-1821-4_1,

1.2 Background

1.2.1 Terahertz Radiation

The terahertz (THz) part of the electromagnetic spectrum lying between the millimeter wave and infrared (100 GHz–10 THz) bands is of significant importance to the biological sciences because complementary information to traditional spectroscopic measurements on low-frequency bond vibrations, hydrogen bond stretching, and bond torsions in liquids and gases may be obtained. The vibrational spectral characteristics of biomolecules, which lie in this range (wavenumbers between 3.3 and 333 cm^{-1}) make T-rays a promising sensing modality for clinical diagnosis. Since THz photons, (or T-rays), have significantly lower energies (e.g., only 0.04 MeV at 100 GHz) than X-rays, they have been considered by many as noninvasive. Although nonlinear interactions between biological tissue and coherent THz radiation have been predicted by Fröhlich (1980) and experimentally verified by the careful work of Grundler and the analysis of Kaiser (Grundler and Kaiser 1992) in the 1990s, the widely held view at the moment is that any measurement technique that operates at THz frequencies at reasonably low power levels should be considered as noninvasive. Such a conclusion is based on the assumption that in the absorption processes involved, when THz pulses interact with biological tissue, the Gibbs free energy conveyed in the THz light beam is insufficient to drive chemical reactions. For example, the molar energy at a frequency f of 100 GHz would be given from $E = Nhf$, where $N = 6.023 \times 10^{23}\ \mathrm{mol}^{-1}$, (Avogadro's number), and $h = 6.626 \times 10^{-34}$ Js (Planck's constant); the calculated value of only $E = 0.04$ kJ mol^{-1} is so low (approximately 100 times lower than the amount of molar energy required for ATP hydrolysis) that for most practical purposes we may assume that the interference with biochemical processes would be minimal. Figure 1.1 illustrates the different parameters used to describe where the T-ray frequencies, from 100 GHz to 10 THz, lie on the electromagnetic spectrum.

Another advantage of performing imaging based on the optical properties of biological tissue with THz radiation is lower scattering than infrared light. Organ differentiation on the basis of tissue water content using microwave transmission or reflection measurements is impractical because the diffraction-limited minimum spot size for a free-space beam is too large to avoid beam spillover around most tissues and organs. From a technological point of view, THz imaging needs to compete with positron emission tomography (PET) imaging that has picomolar sensitivity but poor spatial resolution and magnetic resonance imaging (MRI) that offers millimolar sensitivity with high spatial resolution. Indeed, a diffraction-limited imaging system operating at 1 THz would have a spatial resolution of 300 μm, which should be considered sufficient for many biomedical applications. Meanwhile, since 70% of the human body is composed of water, a large part of the energy in the excitation pulse is attenuated, and the resultant patterns of many biomedical samples can be identified via applying advanced signal processing techniques.

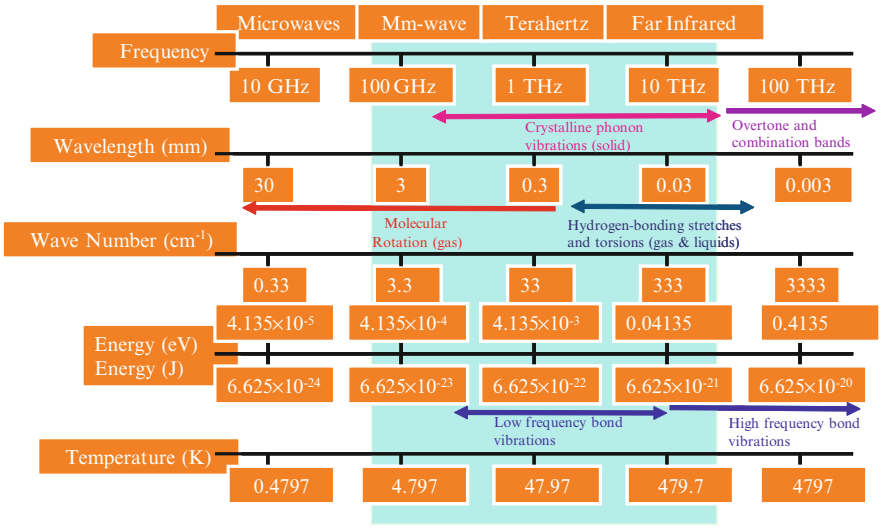

Fig. 1.1 Electromagnetic spectrum. Illustration of electromagnetic spectrum (Figure courtesy of Sillas Hadjiloucas, Department of Cybernetics, The University of Reading, Reading, UK)

1.2.2 THz Pulsed Imaging and Continuous-Wave Imaging

In this book, terahertz pulsed imaging (TPI) and continuous-wave (CW) THz quantum cascade laser (QCL) imaging are utilized, for example, THz experiment data sets. Following (Karpowicz et al. 2005a), the comparison between the two different types of imaging is listed here to highlight their respective strengths and weaknesses.

First, we highlight the differences in hardware. Regarding the pulsed THz imaging system, a standard pump-probe setup using a femtosecond pulse laser is used. A photoconductive antenna (PCA) or a nonlinear crystal through optical rectification is used as a terahertz emitter. The THz response is detected via PCA device or electrooptic sampling (EOS) driven by optical probe pulses. A CW THz imaging system may apply purely electronic sources, for example, the Gunn diode, without involving a pump-probe setup and a time delay scan. Photomixing techniques may be used in the emission and detection of terahertz radiation. QCLs and backward wave oscillators also allow for generation of THz radiation. In order to recover depth resolution of target measurement, a THz CW imaging system does this at the cost of decreased SNR Karpowicz et al. (2005a). Interferometry is used to recover phase information, and multiple or tunable sources with sufficient frequency range allow recovery of frequency-domain information.

Differences in data acquisition between CW and pulsed systems motivate us to develop different algorithms for tomographic reconstruction. Pulsed THz time-domain imaging affords data richer in information but may require more advanced

processing techniques. Depth information can be recovered from pulse timing. The temporal location of the reflected peak indicates a change in the optical path length, and the time delay between these reflected pulses and the main pulse can easily be converted to depth. For a CW THz imaging system, in the form of a raster, intensity image data are yielded if only a fixed-frequency source and a single detector are involved.

1.3 Morphology Outline

This chapter introduces T-ray biosensing and the key areas presented in this monograph, while Chap. 2 reviews the literature on T-ray generation and detection. Chapter 3 reviews terahertz imaging modes, which are the platforms to achieve THz pattern recognition, which is presented in Chap. 4. These chapters provide a survey of the state of most current research in the THz field. These reviews offer new perspectives on THz issues and identify areas in need of further research.

Chapter 5 develops a pattern recognition framework for the identification of materials in pulsed THz images. Chapter 6 presents a review of the theory and practical techniques regarding the application of wavelets to signal and image analysis. Wavelet soft threshold denoising is also demonstrated in this chapter, which attempts to isolate material information present in the THz waveforms from systematic and random noise data. It is shown that this contributes to improvements in THz pattern recognition system performance. Chapter 7 describes five feature extraction algorithms for the resolution of different THz pattern recognition applications. In particular, ARMA models for wavelet subband coefficients form one of a few novel contributions in this monograph. The final step for pattern recognition introduces the classifier, which is discussed in Chap. 8. Several popular classification schemes are reviewed in this chapter. A number of THz case studies concerning THz pattern recognition with application of the represented pattern recognition framework and relative algorithms are illustrated in Chap. 9.

Radon transforms for tomographic reconstruction are introduced in Chap. 10. This chapter combines traditional computed tomography (CT) with conventional THz imaging. The reconstruction formulae are expressed in both the time and frequency domains. A novel segmentation technique using 2D wavelet transforms is illustrated in Chap. 11, where polyethylene samples are used to achieve reconstructed tomographic images and extracted segments corresponding to different media. Chapter 12 highlights a local tomographic reconstruction of THz measurements using wavelets, with aims to reduce measurement time in practical application. Chapter 13 further applies the local reconstruction algorithm on CW THz QCL imaging. The optical properties of the QCL on a cubic sample with complex contours are explored.

In the case of pulsed THz tomography, our rationale for the use of wavelets is that both THz pulses and wavelets are time localized—this matching results in a small

number wavelet coefficients with high signal power, whereas noise is nonlocalized, and thus, noise power is thinly spread over many wavelet coefficients. However, in Chap. 13 where we adopt CW THz tomography, the rationale is mainly that short wavelet filters have good 2D localization in the computed DWT, which limit the spatial extent of reconstruction artifacts. As in the CW case, we are considering *local* reconstruction; we highlight that the wavelet localization feature is advantageous for zooming into the finer details for local reconstruction.

Chapter 14 concludes the monograph with a summary of its highlights, and recommendations for extending T-ray pattern recognition and computed tomographic (CT) reconstruction in the future.

Appendix A introduces the oblique projection operation. It is important to understand subspace system identification algorithms. Appendix B provides further details about back-projection algorithms. Appendix C details on error analysis with respect to wavelet-based local reconstruction. Appendix D contains the details and specifications of the components of both the pulsed THz imaging hardware and CW terahertz imaging QCL hardware, utilized in this monograph. Appendix E lists some of the key algorithms for the realization of THz pattern recognition tasks and CT reconstruction. These are used for THz data analysis.

1.4 Original Contributions

This monograph highlights a number of useful techniques in the area of THz science and technology.

On the material identification front, a classification framework for THz spectroscopy is described. This framework encompasses preprocessing, feature extraction, and classification techniques. The denoising of terahertz signals by modifying wavelet transform coefficients (discrete wavelet transforms and discrete wavelet packet transforms) is illustrated with experimental data (Sects. 6.5 and 9.2.4.1). Three feature extraction algorithms are discussed. The first uses statistical modeling (AR/ARMA) using wavelet coefficients to extract highly descriptive features, represented in Sect. 7.4. The second uses oriented frequency components as classification features, illustrated in Sect. 9.5.2. The third is to apply system identification for feature extraction, consisting of subspace and wavelet packet algorithms (Sect. 7.5). Three classifiers are applied for the final evaluation of classification, including Mahalanobis classifier (Sect. 8.1), the Euclidean discrimination matric (Sect. 8.2), and the support vector machine (SVM) (Sect. 8.3).

Finally, several experimental case studies are conducted to illustrate the performance of the classification framework. The identification of cellular differences between normal human bone cells and human osteosarcoma cells is demonstrated in Sect. 9.4.1, two-class RNA patterns and multiclass terahertz pulses are studied in Sect. 9.5, and the identification of lactose and mandelic acid THz spectra is overviewed in Sect. 9.3.

The goal of THz material identification via a classification framework, is to achieve a quantitative representation of THz spectroscopy. The goal of THz CT reconstruction is to achieve a description of the complete target of interest (Duda et al. 2001) via applying T-ray imaging measurements of the whole object. Chapter 11 represents a novel segmentation technique, which is derived based on THz pulsed (i.e., broadband) CT reconstruction. According to the fact that with the incremental wavelet scale, noise is reduced and the target intensity (energy) is increased in an image, it turns out that, after extracting the low-frequency 2D subband of fused T-ray CT images, an increased signed energy with an increase in wavelet scale is used as a cue to extract the target regions.

Terahertz computed tomography (THz-CT) is a form of coherent tomography. For time-domain terahertz measurements, it is impractical to achieve full exposure data for only local reconstruction of the subregion of interest (ROI). In order to overcome the ill-posed inverse problem from traditional filtered back-projection (FBP) algorithms, we apply a wavelet-based algorithm to reconstruct THz-CT images with a significant reduction in the required measurements when the ROI is small. The algorithm recovers an approximation of the ROI from terahertz measurements within its vicinity, and thus improves the feasibility of using terahertz imaging to detect defects in solid materials and diagnose disease states for clinical practice, etc. This is presented in Chap. 12.

The local reconstruction of the ROI from a 3D terahertz imaging is obtained via a QCL, illustrated in Chap. 13. It is an important step in the understanding wavelet-based techniques and traditional filtered back projection (FBP) to map terahertz local measurements for resolution. In this example, a clown's head (made of polystyrene), with a hole inside with complex contours, is used as a sample to explore the ability of a QCL to image target object with complex contours. The resultant analysis has shown that wavelet-based reconstructions offer robust reconstruction performance in the local reconstructed shape of the target. Fuzzy *c*-means (FCM) segmentation (Chuang et al. 2006) is used in post-processing to make measurements on the target's internal structure, which provides an iterative measurement to minimize the classification error allowing each pixel to be the member of all the possible classes with varying membership.

Perhaps the most significant highlight is the realization of wavelet-based T-ray local CT. This technique is validated via both THz broadband (pulsed) and narrowband (CW) tomographic imaging schemes. The latter uses an advanced THz QCL emitting at 2.9 THz housed at the University of Cambridge. The THz QCL is a GaAs-AlGaAs bound-to-continuum superlattice design and is mounted on the cold finger of a continuous-flow helium-cooled cryostat. By contrast with TPI, QCLs afford high-power sources of CW radiation to achieve deeper penetration of samples. From the mathematical derivation point of view, the development of reconstruction algorithms is to combine together the separate wavelet transforms and ramp filters, which forms an improved version of traditional FBP. This is because the traditional filter back-projection algorithm introduces a discontinuity in the derivative of the Fourier transform at zero frequency. This means that

the traditional Radon transform inversion does not allow a complement of local reconstruction of a CT image. The wavelet-based algorithm used in this monograph realizes actual *local* THz tomographic reconstruction. It turns out to be a rapid tomographic reconstruction with reduced measurement time.

These areas advance the goal of the development of practical 3D THz inspection systems. They provide substantial improvements over the existing state-of-the-art and serve to extend THz applications to new and potentially ground-breaking realms.

Chapter 2
Terahertz Sources and Detectors

This chapter describes techniques and systems regarding terahertz sources and detectors, mainly reviewing basic concepts and principles to help understand THz imaging instruments. The terahertz technologies outlined in this chapter provide background knowledge to the experimental work on the identification and reconstruction of terahertz spectroscopic data introduced later in this monograph. This chapter also covers the imaging modes, which involve both ultrafast pulsed systems and terahertz QCLs.

2.1 Introduction

Terahertz science has become increasingly popular in the recent decade due largely to the advent of time-domain spectroscopy (TDS) with ultrashort-pulse laser sources, which makes it possible for researchers to carry out time-resolved "far-infrared" (FIR) studies and to explore spectroscopy and imaging applications in the submillimeter wavelength regime.

Terahertz phenomena follow fundamental scientific interests. The goal of this chapter is to review the basic principles of different types of terahertz sources and detectors that are now possible with terahertz spectroscopy. They are fundamental to the understanding and conducting of the terahertz experiments, described later in the monograph.

This chapter will be organized as follows. Section 2.1 briefly introduces the history of terahertz radiation. Section 2.2 describes basic solid-state lasers, which are the principle components to achieve pulsed and continuous modes of terahertz spectroscopy. The topics range from conversion of ultrafast free-space laser pulses, to free-electron lasers (FELs), as well as QCLs. Section 2.3 introduces hardware devices for generating terahertz radiation. These terahertz emitters include EO emitters, PCA, planar antennas, and magnetic field enhancement devices, along

X. Yin et al., *Terahertz Imaging for Biomedical Applications: Pattern Recognition and Tomographic Reconstruction*, DOI 10.1007/978-1-4614-1821-4_2,

with terahertz photomixing. Section 2.4 discusses different types terahertz receivers based on different optical sampling methods. EO versus photoconductive and synchronous versus asynchronous sampling techniques are investigated.

2.2 The History of T-Rays

The term *terahertz* gained popularity among spectroscopists during the mid-1970s, (Kerecman 1973; Ashley and Palka 1973; Fleming 1974; Siegel 2002). A decade later, as a result of the efforts of many researchers and scientists, advanced techniques in optical rectification and photoconduction had been developed (Auston 1983; Smith et al. 1988) (see Sect. 2.4). These techniques made it possible to produce THz radiation directly using multimode lasers (van Exter et al. 1989; Cantor et al. 1981), such as Ti:sapphire-based lasers and FELs (Sect. 2.3.1). In 1989, Martin van Exter introduced a terahertz time-domain spectroscopy (THz-TDS) system (van Exter et al. 1989). This added momentum to the field of T-ray generation and detection, and some simple research began, including the extraction of material parameters from THz-TDS measurements.

Following this, Hu and Nuss in 1995 used a traditional scanned imaging system to acquire two-dimensional (2D) images. This was the beginning of geometric image formation of an object in the T-ray frequency range. TPI was viewed as a novel and promising method, especially applied to medical diagnostics (Löffler et al. 2001).

Subsequently, much effort was devoted to system improvement (Löffler et al. 2002). This included progress toward wavelet denoising of terahertz pulse imaging data (Ferguson and Abbott 2001b), denoising techniques for terahertz responses of biological samples (Duvillaret et al. 1996; Ferguson and Abbott 2001a), reducing measurement time (Zhao et al. 2002), and improving spatial (Chen et al. 2000) and depth resolution (Johnson et al. 2001). Improved systems made possible the development of new systematic approaches, such as time resolution of TPI in translation and reflection mode (Mittleman et al. 1997), dark-field TPI (Löffler et al. 2001), THz pulsed near-field image with good spatial resolution (Federici et al. 2002; Schade et al. 2004). In turn, T-ray CT technology was applied (Wu et al. 1996; Jiang and Zhang 1998a; Ferguson et al. 2002c,b). A review of further imaging modalities can be found in Chap. 3.

In the last 5 years, the rapid improvement of T-ray detectors and sources resulted in many technical advantages in THz-TDS and therefore opened up new fields of application. In particular, T-ray pulsed technology was used to image opaque objects. One promising application is the inspection of biomedical tissue. Examples are the separation of tumor cells from normal tissue (Woodward et al. 2002) ex vivo, and the study of in vivo normal to pathological samples of human skin (Gladkova et al. 2000), three-dimensional detection of tooth decay (Arnone et al. 2000), together with optical imaging and classification of a bird head (Löffler et al. 2002). Further aspects of spectroscopy and image analysis are reviewed in Chap. 4.

Time-domain TPI has the advantage of providing a broad frequency spectrum, but it incurs the high cost of an expensive femtosecond laser. CW imaging is attractive since it is a tunable, compact, and cost-effective system.

A coherent all-optoelectronic THz measurement system via photomixing techniques is normally implemented to produce tunable CW THz radiation. It was first demonstrated in 1998 by Verghese et al. (1998). Following this, Gu et al. (1999) pointed out that a tunable dual-wavelength external cavity laser diode was a promising laser source for the generation of tunable CW-THz radiation. Phase-sensitive CW THz imaging using diode lasers was introduced in 2004, with image capture rates comparable with those from state-of-the-art pulsed THz systems (Gregory et al. 2004). These diode lasers are cost effective for producing CW THz radiation. Additionally, Siebert et al. (2002) used two-color Ti:sapphire lasers to generate CW T-rays with an extension to biomedical applications. However, there exists an obvious drawback in that two expensive Ti:sapphire laser sources are required. The CW THz radiation mentioned above is generated by applying a pair of laser sources and photomixing techniques to achieve a tunable frequency range. For comparison, an entirely electronic generation and detection scheme is illustrated by Karpowicz et al. (2005b) and is a relatively compact CW THz imaging system with a few components. Such a system could easily be made portable, thus opening a much wider range of possible applications. However, as it lacks depth and phase information, the system only yields two-dimensional intensity images.

Photomixing techniques (in Sect. 2.4.3) applied to the generation of CW terahertz radiation, very severely limit the output power to $\sim 1\,\mu W$ at frequencies above 1 THz (Kim et al. 2006) mainly because of intrinsic parasitic impedance of the device and the impedance mismatch between the device and the radiating antenna (Darmo et al. 2004). QCLs operating in the terahertz range, however, have remained elusive for a long time until 2004, when the first terahertz QCLs were reported (Köhler et al. 2001). This is because of an insuperable barrier that exists in the phonon *reststrahlen* band, which causes difficulty in the further expansion to lower emission terahertz frequencies. Further, the development of a suitable waveguide is necessary (Sirtori et al. 1998a). It aims to confine light of the long wavelength within terahertz range to an epilayer compatible with molecular beam epitaxy technology and with low absorption losses onto the laser mode (Tredicucci et al. 2005). Recent novel design concepts have led to CW operation and high output powers (Rochat et al. 2002). In the recent years, terahertz QCLs have made rapid progress. They depend on chirped superlattices (Köhler et al. 2002a) and the surface plasmon concept (Köhler et al. 2002b) employed for a large optical confinement with low propagation losses, to recently, bound-to-continuum transitions and extraction of carriers via resonant phonon scattering (Williams et al. 2003). The lowest emission frequency is now ~ 1.39 THz. More recent progress of QCLs in terahertz range is presented in Sect. 2.3.3. One of considerable advantages of QCLs is the ability to tune the terahertz source to avoid regions of high water absorption. A relevant experiment has been conducted (Lee et al. 2006) with the atmospheric window selected at ~ 4.9 THz, to achieve real-time imaging of a dried seed pod at a 25-m

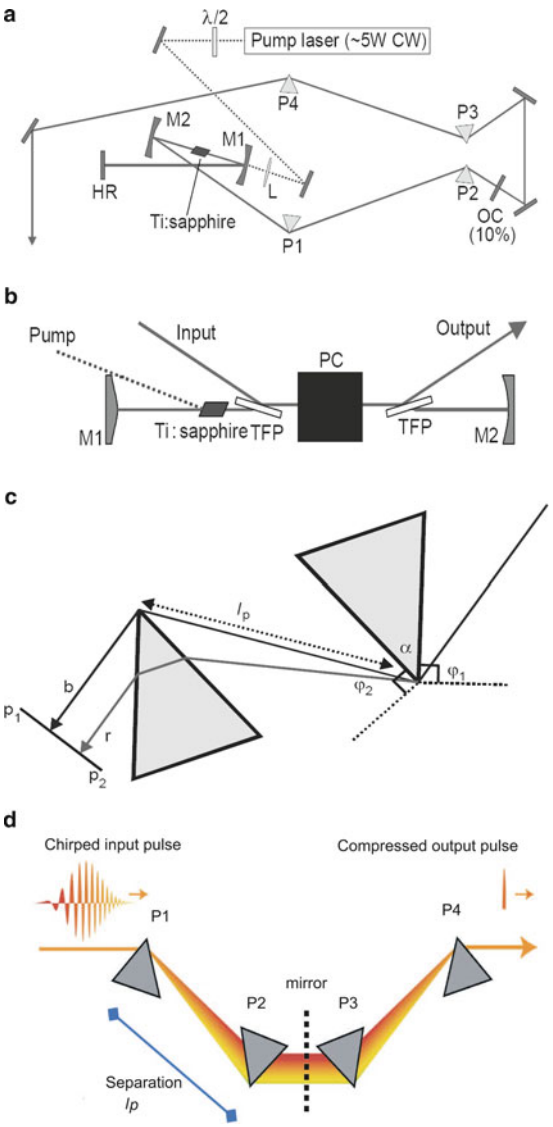

Fig. 2.1 Ti:sapphire-based lasers. (**a**) Diagram of a basic self-mode-locked Ti:sapphire oscillator shows the cavity layout. The output pulse is output from the end of the cavity dispersion, and then is tuned by a pair of matching extracavity prisms. (**b**) The schematics for regenerative amplification in Ti:sapphire oscillator. Ti:sapphire rod, 5 mm or less in length, is doped to absorb about 90% of the incident pump radiation. Two concave focusing mirrors, a pair of Kerr lenses, allow passive mode locking, where M1 is a high reflector and M2 is an output coupler. This pair of Kerr lenses forms the optical cavity. When light travels between the two lenses, the energy is accumulated in the interval of the gain medium, which causes a population inversion. The TFP indicates a thin-film polarizing beam splitter. The Pockel's cell (PC) is a Q switch and consists of voltage-controlled wave plates. The voltage rotates the plane of polarization by 90°, which results in the light being able to pass the medium. If the laser is Q-switched, a brief burst of light

standoff (see the relevant image mode in Sect. 3.2.3). Another important application of terahertz QCLs is in biomedical imaging; this is well illustrated by the work of Darmo et al. (2004) in imaging a rat brain section at 3.4 THz (Sect. 4.2.2).

Emission of relatively strong CW terahertz radiation from cuprate superconductors is carried out by Ozyuzer et al. (2007). Josephson junctions are stacked within the layered high-temperature superconductors. It is an important step toward filling this "terahertz gap" from 0.5 to 1.4 THz, in which the photomixing techniques and QC lasers can barely reach.

2.3 Laser Sources

2.3.1 Ti:Sapphire-Based Lasers

Ti:sapphire-based lasers were revolutionized in the 1990s, with the invention of self-mode-locking techniques. Currently, it is one of the most important laser sources for generating terahertz radiation (Reid and Fedosejevs 2005). Ti:sapphire-based lasers are frequently applied for the generation of pulsed terahertz radiation.

The principle of a Ti:sapphire-based laser is simply presented as follows. It consists of a rod of Ti:sapphire (titanium-sapphire), which can be pumped by a CW laser source. This light is focused into the Ti:sapphire rod collinearly with the laser axis through the back of a lightly silvered mirror. Dispersion arises from the variation of the refractive index of the crystal material across the gain bandwidth of the laser. The cavity dispersion output from the crystal material is Q-switched and self-mode-locked with the use of a pair of Kerr lenses (Brabec et al. 1992) as a saturable absorber and a Pockel's cell modulator. The schematic diagram regarding the Ti:sapphire pulsed laser oscillator is illustrated in Fig. 2.1b. The output from the laser oscillator, in Fig. 2.1a, is taken from the end that is opposite the dispersion-compensating prisms. This alignment of the prism pair creates a longer path for red wavelengths propagating through the prism material, as compared with the blue, which yields a negative dispersion effect. It is illustrated in Fig. 2.1c. If the prism separation, lp (defined tip to tip), is sufficiently large, the positive dispersion of the material can be balanced. The prism apex angle is cut to guarantee that at minimum deviation of the center wavelength, the incident angle is the Brewster

Fig. 2.1 (continued) excites population inversion and produces a stronger pulse. (**c**) Prism pairs are used in the control of dispersion; r and b indicate the relative paths of arbitrary long- and short-wavelength radiation. The incident (Brewster) angle at the prism face is labeled by φ_1. The light is reflected in the plane $p_1 - p_2$ in order to remove the spatial dispersion. (**a**)–(**c**): After Reid and Fedosejevs (2005). (**d**) Illustration of the optical path of the output cavity dispersion through the prism pairs. After Kafka and Baer (1987)

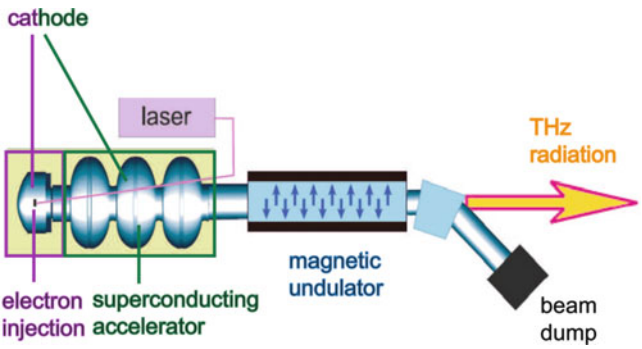

Fig. 2.2 A schematic of a THz free-electron laser. The schematic shows a short injector-accelerator combination compared to a stand FEL. After Grosse (2002)

angle. Figure 2.1d shows the optical path of the output cavity dispersion through the prism pairs. The compressed output pulse is finally achieved from chirped cavity dispersion by the application of prism pairs. The photograph of a Ti:sapphire-based laser is shown in Appendix D in Fig. D.1.

2.3.2 Free-Electron Lasers

Terahertz free-electron lasers (FELs) feature high intensity, combined with short pulse length, easy tunability, and variable pulse structure. These features are essential for biological and medical studies (Grosse 2002) and for the exploration of vibrational and configurational molecular transitions (Kato et al. 2000; Xie et al. 2002) in terahertz regime.

Unlike femtosecond lasers, that is, Ti:sapphire-based lasers, where quantum-mechanical principles are employed, the FEL (Krishnagopal et al. 2004) is a classical laser and converts part of the kinetic energy of the electrons into coherent electromagnetic radiation.

Figure 2.2 shows a schematic of a terahertz FEL. Two major components of the device are: electron accelerator and undulator. Generally, an undulator, such as in a linac or a synchrotron, is used to produce magnetic fields, which then drive an electron beam from an accelerator to achieve coherent terahertz pulsed radiation. Different from the setup of conventional FELs, the terahertz FELs accelerate electrons directly after they leave the photocathode (Volkov et al. 2000). The realization of a compact table-top full terahertz FEL system is now possible (Grosse 2002).

2.3.3 Terahertz Quantum Cascade Laser

Recent advances in nanotechnology have also led to the development of semiconductor-based THz sources: the terahertz QCL (Tonouchi 2007). Terahertz radiation is generated when electrons propagate the serial connection of coupled quantum wells. Quantum wells are formed in semiconductors by having a material, like gallium arsenide sandwiched between two layers of a material with a wider bandgap, such as $Al_xGa_{1-x}As$. These structures can be grown by molecular beam epitaxy with choice of the layer thickness, which determines the electron wave functions of the subbands. Unlike the conventional bandgap structure of semiconductor lasers, in QCLs, quantum confinement splits the conduction band into a number of distinct subbands (Köhler et al. 2002b; Faist et al. 1994). The energy spacing of the lasing subbands determines the radiation frequency, allowing in principle to produce light at arbitrarily long wavelengths.

Since the first QC laser was demonstrated at the much shorter wavelength of 4 μm (75 THz) at Bell Labs in 1994 (Faist et al. 1994), there have been over five types of terahertz QCLs since, due to the different mechanisms of electron energy relaxation processes (Vitiello et al. 2006). They are "chirped superlattice" (Williams 2007; Köhler et al. 2002b), "interlaced" (Köhler et al. 2004), and "resonant phonon" (Williams et al. 2004), "bound-to-continuum" (Vitiello et al. 2006) laser, as well as a recent design of two-color QCL with application of a magnetic field (Scalari et al. 2006).

The first THz QC laser with a photon energy less than the semiconductor optical phonon energy was demonstrated at 4.4 THz (equivalent to a wavelength of 67 μm) by Köhler et al. (2002b). A chirped superlattice (SL) technique was adopted to design the QCL active region, with advantage of very large current-carrying capabilities and optical powers (Tredicucci et al. 1998).

The bound-to-continuum (BTC) QCL has been proved to be successful in producing terahertz radiation with the replacement of the original chirped SL (CSL) design (Köhler et al. 2002b). The bound-to-continuum QCL takes place between an isolated upper state and a miniband with a small well adjacent to the injection barrier (Faist et al. 2001). The design combines the advantages of the three QW and superlattice active regions. It makes it possible to achieve selective injection into the upper state and fast extraction from the lower state. As a result, these designs display improved temperature and power performance compared with the CSL designs (Williams 2007; Alton 2005). A relevant experiment to use a BTC QCL for wavelet-based local reconstruction of a 3D polystyrene object is represented in Chap. 13. Figure 2.3a illustrates the design and performance of a bound-to-continuum QCL emitting at 2.9 THz. The laser was made at the University of Cambridge, by Jesse Alton, in collaboration with his colleagues (Alton 2005). The QC structure was grown by molecular beam epitaxy in a $GaAs/Al_{0.15}Ga_{0.85}As$ material system on a semi-insulating GaAs substrate. One period of the conduction band profile for each active region is displayed along with the calculated moduli squared of the most relevant wave functions.

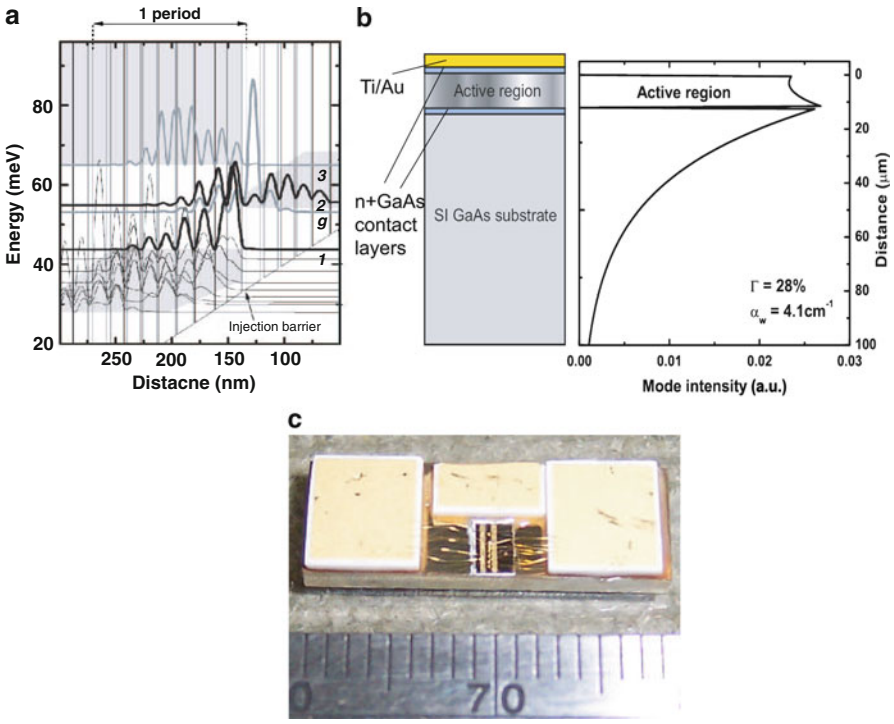

Fig. 2.3 The terahertz BTC quantum cascade laser scheme. (**a**) One period of the conduction band profile regarding a "vertical transition" design of the layer sequence. The upper, and lower state of the laser transition and the injector miniband ground state are labeled 2, 1, and g, respectively. The transition energy, given by the energy difference between 2 and 1, is 12 meV. At alignment, the wave functions of the upper and lower state are broadly overlapped. The upper state wave function is concentrated mainly in the two quantum wells adjacent to the injection barrier, reducing the overlap with the lower energy states in the injector miniband, thereby enhancing the non-radiative upper state lifetime. Electrons are injected into the upper state from state g through the injection barrier. The active region consists of 85 identical repeat periods. (**b**) Schematic representation of completed wafer cross section (*left*) and computed optical mode profile (*right*) along the growth axis. This waveguide is shown at $\lambda = 103\,\mu\text{m}$ (12 meV) and the yielded waveguide losses (α_w) of 4.1 cm^{-1} and a confinement factor (τ) of 28%. After Alton (2005). (**c**) Photograph of the BTC QCL (Figure courtesy of Lynn Gladden, Department of Chemical Engineering, The University of Cambridge, Cambridge, UK)

Figure 2.3b illustrates the waveguide design of the two BTC QCLs emitting at 2.9 THz. Both active regions are embedded between identical cladding layers: top contact layer is an 80-nm-thick GaAs, and bottom contact layer is a 700-nm-thick GaAs. The two contact layers are designed regarding the surface plasmon waveguide. The former has the same mode as a quasi-metallic layer (Köhler et al. 2002b) and the latter is completed by a Ti/Au metallization layer on top of the ridge cavity (the top contact layer). Figure 2.3c shows the photography of the finished BTC QCL.

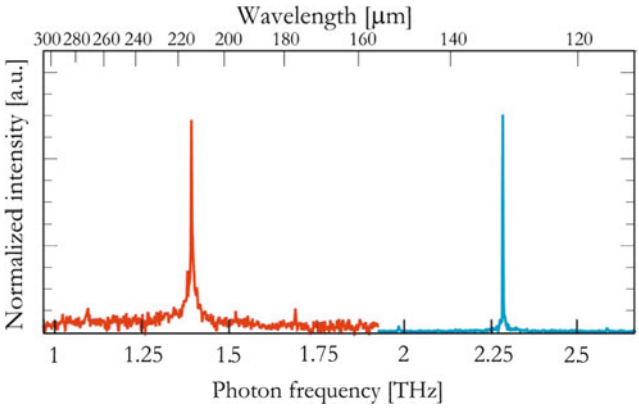

Fig. 2.4 Two-color terahertz quantum cascade laser spectrum. Illustration of the measured spectrum depending on the applied magnetic field. The line on the right indicates the emission frequency of 2.3–2.36 THz, and the line on the left corresponds to the emitted laser frequency at 1.39 THz. After Scalari et al. (2006)

In addition, a THz QCL utilizing alternating photon- and phonon-emitting stages has been developed to achieve efficient extraction of electrons from the lower laser level (Köhler et al. 2004). Though the impact of this interlaced photon–phonon cascade laser has been limited, they are particularly notable for achieving very long wavelength operation (Williams 2007). The other major active region type is the resonant-phonon (RP) scheme. The key design is to use resonant LO-phonon scattering to selectively depopulate the lower radiative level, while maintaining a long upper level lifetime. Owing to the lack of a miniband, the RP designs tend to have smaller oscillator strength (Williams et al. 2004).

At present, a QCL emitting at as low as 1.39 has been demonstrated by Scalari et al. (2006). An electrically switchable, two-color QCL emitting at 1.39 and 2.3 THz is realized by multiwavelength operation. A magnetic field is applied perpendicularly to the layers to increase the gain enabling laser action. The structure is based on a large single quantum well, and multi-wavelength operation is obtained by selectively injecting carriers via resonant tunneling into one of the excited states of this large quantum well (Sirtori et al. 1998b). Figure 2.4 shows the measured spectrum depending on the applied magnetic field.

2.4 Terahertz Semiconductor Sources (THz Emitters)

All-optical techniques have been recognized as an alternative approach to produce THz radiation (Davies et al. 2002) owing to the difficulties in fabricating solid-state THz sources. Semiconductor surfaces are widely used in conjunction with femtosecond visible/near-infrared lasers as THz emitters. Bulk EO rectification (difference frequency mixing) and ultrafast charge transport techniques have been